Apparatus to measure relativistic mass increase

John W. Luetzelschwab
Department of Physics and Astronomy, Dickinson College, Carlisle, Pennsylvania 17013

(Received 4 September 2002; accepted 28 January 2003)

An apparatus that uses readily available material to measure the relativistic mass increase of beta particles from a radioactive ^{204}Tl source is described. Although the most accurate analysis uses curve fitting or a Kurie plot, students may just use the raw data and a simple calculation to verify the relativistic mass increase.
[DOI: 10.1119/1.1561457]

I. INTRODUCTION

Although relativity is a standard topic in the physics curriculum, students generally do not have an opportunity to experimentally verify either time dilation or mass increase. One experiment[1–4] uses the Compton effect to verify the relativistic mass-energy relationship. However, this type of experiment requires a gamma detector, a multichannel analyzer, and several gamma radiation sources.

Another experimental method uses a radioactive source, two strong magnets, and a particle NaI detector.[5] However, this experiment requires a ^{90}Sr source with an activity of about 25–30 μCi, considerably greater than the 0.1 μCi allowed for possession without a Nuclear Regulatory Commission (or state) license. Most academic institutions do not have access to the required source and therefore are not able to perform this experiment.

The apparatus described in this paper is similar to the second experiment, but uses a 10 μCi ^{204}Tl radioactive source that does not require a license and a Geiger Mueller (GM) detector rather than a particle NaI detector. These features and the availability of large [10.2 cm by 15.2 cm by 2.5 cm ($4''\times6''\times1''$)] ceramic magnets mean that most academic institutions can build this apparatus with readily available equipment and at moderate expense.

This experiment is ideally suited for use in a modern physics course as a way to provide experimental evidence for the theory of relativity. Dickinson College sophomore modern physics students used this apparatus in the spring of 2002. In addition, students in five previous classes used an earlier version.

II. THEORY

A charged particle moving in a magnetic field experiences a force perpendicular both to the direction of the velocity and to the direction of the magnetic field. Therefore a charged particle moving in a uniform magnetic field has a circular path with the magnetic force supplying the centripetal force. If we equate these two forces, we have

$$qvB=\frac{mv^2}{r}. \tag{1}$$

The solution for the momentum, mv, is

$$mv=qBr. \tag{2}$$

Therefore, a measurement of the radius of the circular path is a measure of the momentum and the energy.

If all the beta particles from a radioactive nucleus had the same energy, all the particles would have the same radius. However, because a beta particle shares the decay energy with a neutrino (or anti-neutrino), the beta particles have energies that range from zero to the decay energy (or Q-value), and only a very small fraction have the maximum energy. Figure 1 shows a typical beta energy spectrum.[6] This plot does not include the Fermi function, which accounts for the deceleration of the emitted β^- particles (or acceleration of β^+ particles) as they travel through the atomic electrons.

Because the number of beta particles having the maximum energy is very small, the number of counts recorded at the radius of the maximum energy particles is not distinguishable from the background. Only at a smaller radius does the detector measure appreciable counts above background. Therefore, to determine the exact radius of the maximum energy particles, students must extrapolate from the counts at small radii to determine where the counts would decrease to zero at some larger radius.

Figure 1 also shows that the beta energy spectrum is not linear when the kinetic energy, K, approaches the Q-value so a linear fit to the data does not give a good extrapolation. In addition, the plot of counts versus r is a plot of counts versus momentum and not versus energy. Therefore, to plot the data as a function of radius, the students must use the momentum equation for a beta spectrum. The number of beta particles as a function of momentum is[6]

$$N(p_e)\propto p_e^2(Q-K)^2F(Z',p_e^2)|M_{fi}|^2S(p_e,p_v), \tag{3}$$

where Q is the decay energy of the nucleus, K is the kinetic energy of the particle ($[(p_ec)^2+E_0^2]^{1/2}-E_0$), E_0 is the rest mass energy of an electron, $F(Z',p_e^2)$ is the Fermi function with Z' the nuclear charge of the progeny nucleus, $|M_{fi}|^2$ is the nuclear matrix element, and $S(p_e,p_v)$ is the shape factor. The shape factor accounts for the dependence on the momentum of the beta particle (p_e) and the anti-neutrino (p_v) in forbidden transitions.

The Fermi function accounts for the fact that the atomic electrons slow the emitted β^- (or accelerated β^+) particles as they pass through this region of negative charge. This function is complicated, but it primarily affects the low energy region of the spectrum. Hence, for this experiment (which is only concerned with energies near $K=Q$), it can be considered a constant.

The decay of ^{204}Tl is a spin 2^- to 0^+ transition, which makes it a first forbidden transition (the beta/neutrino pair carries off $1\hbar$ of angular momentum), so the $S(p_e,p_v)$ factor must remain. The shape factor is given by[6]

$$S(p_e,p_v)=p_e^2+p_v^2. \tag{4}$$

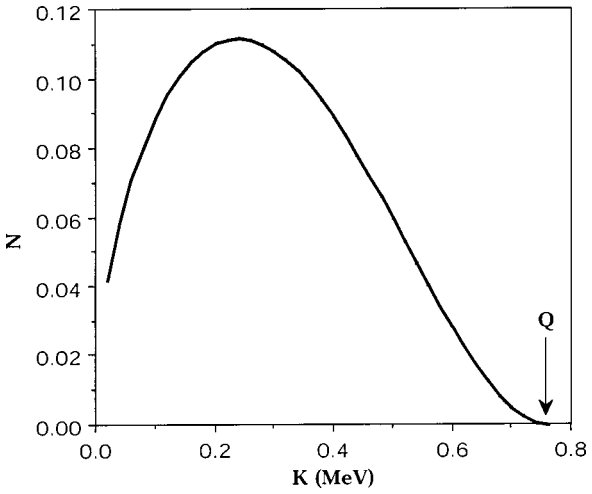

Fig. 1. Plot of the relative number of beta particles versus energy from a ^{204}Tl source. The vertical scale is arbitrary. The plot does not include the Fermi function, which affects the low energy part of the spectrum.

With these adjustments, Fig. 2 shows the beta spectrum from Eq. (3) as a function of momentum.

When students plot the counts versus momentum, they have three ways of determining the maximum momentum or energy of the particles. The easiest way is to just draw a line through their data following the shape of the curve in Fig. 2, thus yielding a maximum momentum value. Another option is to fit the data to Eq. (3) with a curve fitting routine. However, it is better if the variable is K, that is, all momentum terms are replaced by $p=(1/c)[(K+E_0)^2-E_0^2]^{1/2}$), so that the fit gives the maximum energy directly. Also, the students should use only the data points that are close to the maximum energy (but with significant counts above background) so that the Fermi function has a minimal effect.

A more detailed fit uses a Kurie (or Fermi-Kurie) plot. This plot involves the solution to Eq. (3) for $(Q-K)$. The resulting plot of $(Q-K)$ gives a straight line with the intercept at the maximum energy Q. The solution for $(Q-K)$ is[6]

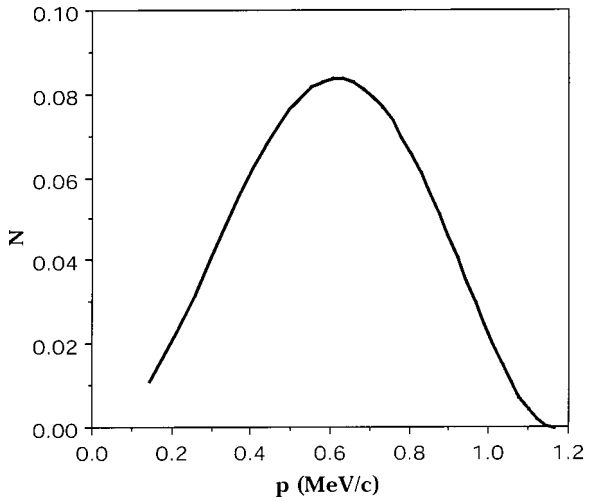

Fig. 2. Plot of the relative number of beta particles versus momentum from a ^{204}Tl source. The vertical scale is arbitrary. The plot does not include the Fermi function, which affects the low momentum part of the spectrum.

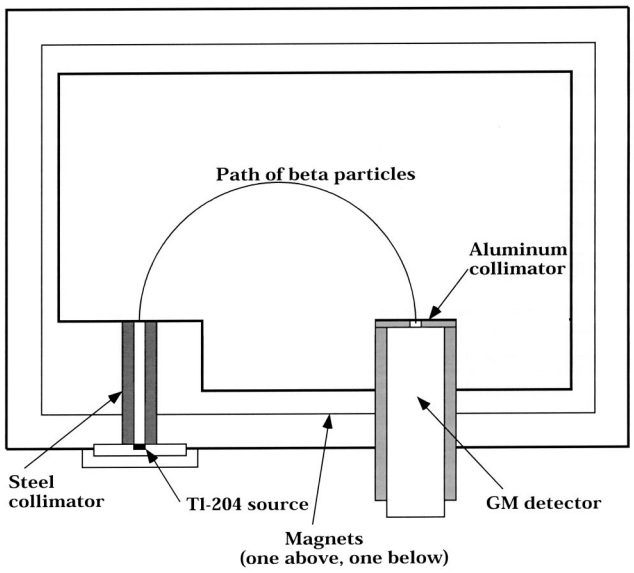

Fig. 3. Sketch of the apparatus used in this experiment. The shaded area represents the area covered by the two magnets. The collimator and detector are located in the gap between the magnets.

$$(Q-K)\propto\left[\frac{N(p_e)}{p_e^2(p_e^2+p_v^2)}\right]^{1/2}, \tag{5}$$

where $N(p_e)$ is the number of recorded counts as a function of momentum (that is, the radius).

The equation for the antineutrino momentum is

$$p_v^2=\frac{E_v^2}{c^2}=\frac{(Q-K_e)^2}{c^2}=\frac{(Q-((p_e^2c^2+E_0^2)^{1/2}-E_0))^2}{c^2}$$
$$=\frac{(Q+E_0-(p_e^2c^2+E_0^2)^{1/2})^2}{c^2}, \tag{6}$$

where E_0 is the rest mass energy of the electron. The substitution of Eq. (6) into Eq. (5) gives the final solution

$$(Q-K)\propto\left[\frac{N(p_e)}{p_e^2(p_e^2c^2+(Q+E_0-(p_e^2c^2+E_0^2)^{1/2})^2)}\right]^{1/2}, \tag{7}$$

where $p_e=qBr$. The plot of Eq. (7) gives the value of Q when $(Q-K)=0$, but it contains the value of Q, which means that we are using the answer to find the answer. However, the intercept depends only weakly on the value of Q in the bracket; using a value 30% below or 30% above the accepted Q value produces only a 0.2% variation in the value of the intercept.

III. APPARATUS

Figure 3 is a sketch and Fig. 4 is a picture of the apparatus. The frame that holds the magnets, source collimator, and detector is made of Lucite. Beta particles from a 10 μCi ^{204}Tl source[7] travel through a steel collimator (0.48 cm inside diameter, 3.02 cm length) until they are in a region of uniform magnetic field. The magnetic field causes the particles to move in a circular path until the particles reach the detector. The detector is a 1.9 cm diameter specially manufactured aluminum casing (that is, nonmagnetic) GM tube[8] with a 1.0 cm diameter sensitive area. All commercially available GM

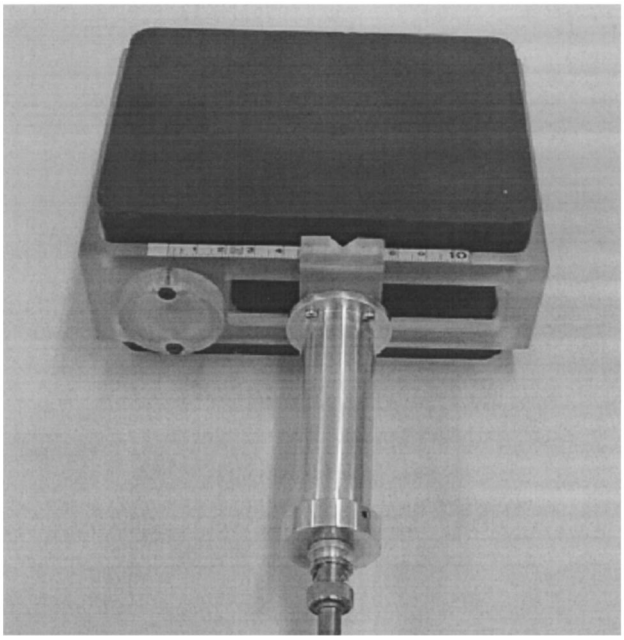

Fig. 4. Picture of the apparatus used in this experiment.

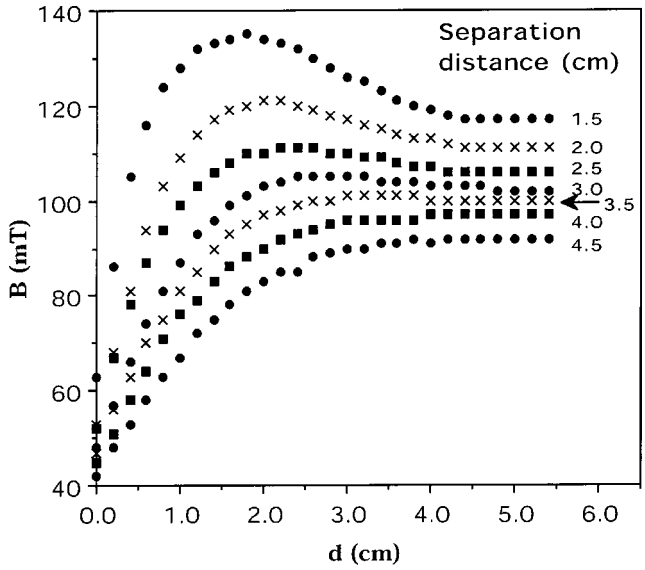

Fig. 5. Plot of the magnetic field in the center of the gap between the two magnets as a function of the distance from the center of the long edge of the magnets.

tubes have stainless steel casings to prevent corrosion by the inorganic gases, so the aluminum tube used in this experiment has an organic gas that has a shorter lifetime than an inorganic gas. However, for the typical counts found in this experiment, the tube will last many years. A 0.16 cm wide collimator in front of the detector limits the detected beta particles to this narrow region. The student moves the detector along the diameter of the circular path to record the number of counts at different radii.

Because the detector collimator subtends a smaller solid angle for particles that travel a longer path, students must determine the solid angle subtended by the collimator at each radius. The solid angle for a radius of 3.5 cm is about 0.001 steradians, so, for convenience, $N(p)$ is reported as the counts per millisteradians.

The basic requirement for this experiment is to have a strong, uniform magnetic field over the path of the beta particles. Large (10 cm by 15 cm) commercially available ceramic magnets[9] provide adequate magnetic fields. However, for one magnet, the field varies between about 0.6 to 0.9 Tesla (T) over the surface of the magnet, with the larger fields being near the edge of the magnet and the small field at the center. This varying field seemingly would produce a nonuniform field between two magnets placed close to each other. However, an investigation of the magnetic field gives some interesting results.

Figure 5 shows a plot of the magnetic field at the center of the magnet gap as a function of the distance from the 15 cm edge of the magnets and for different gap distances. As expected, for small gaps (less than 3 cm), the field reaches a maximum near the edge and then decreases toward the center. For a gap of 1.5 cm between the magnets, the field reaches a maximum of 135 mT at 1.8 cm and then drops to 117 mT at the center, a change of 13%. However, because of the fringing fields at the edges, for gaps greater than 3 cm, the field between the magnets becomes nearly constant for most of the center region.

Although the maximum magnetic field in the gap is desirable, fitting a detector into the gap limits the minimum separation distance. Small end window GM detectors (down to 0.9 cm in diameter) are commercially available; however, the sensitive areas are small, resulting in lower count rates and longer counting times. Based on these data, and a choice of a 1.9 cm diameter detector, the optimum magnet separation is 2.5 cm. For this separation, the magnetic field has a maximum at 2.6 cm and decreases by 5% at the center of the magnet.

The choice of a beta source depends on three factors. First, the progeny nuclei must not have any excited states so that all the decays will have the same maximum energy and the radionuclide will not emit any gamma radiation, which would produce excessive background counts in the detector. Second, the energy must be such that the radius of curvature is appropriate for the magnetic field and size of the constant magnetic field region. Third, the source must be commercially available with an activity that will produce a sufficient count rate. For a 100 mT magnetic field and a maximum radius of less than 5 cm, the maximum energy of the beta particles must be less than 1 MeV, but still be large enough to produce a radius of curvature of 3 to 4 cm. ^{204}Tl, with its 0.76 MeV maximum beta energy, fits these criteria. In addition, it is available in license-exempt 10 μCi quantities.

Other commercially available radionuclides, ^{137}Sr, ^{60}Co, and ^{90}Sr, do not meet the above criteria. For example, ^{137}Cs has two excited states so it emits two maximum energy beta particles and also emits a gamma ray. ^{60}Co, although it emits betas with a single maximum energy, also emits two high-energy gamma rays. ^{90}Sr does not have any excited states, but its progeny, ^{90}Y, is also radioactive and emits a beta particle with a much higher maximum energy, which would have a radius of curvature greater than the 5 cm limit for the magnetic field in this experiment. In addition, the maximum activity of ^{90}Sr that one can purchase without a license is 0.1 μCi, and this activity would not produce a sufficient count rate to allow the experiment to be completed in a reasonable time.

IV. EXPERIMENTAL PROBLEMS

This experiment has several experimental problems. The beta particles travel in air and not in a vacuum so beta particles interact with the electrons in the air and scatter out of their original path. The transmission of monoenergetic electrons through an absorber is approximately a linearly decreasing function of the absorber thickness,[10] but with a smaller slope at small absorber thicknesses. Therefore, the fraction scattered during a short distance in air is less than the ratio of the distance to the range. The maximum-energy beta particle from ^{204}Tl, 0.76 MeV, has a range of 225 cm in air.[11] The semi-circular path length of these particles in this apparatus is πr, which for $r = 3.7$ cm is 12 cm, and hence less than 5% of the maximum energy beta particles are scattered by the air.

The electrons struck by the beta particles gain considerable energy and are detected if they reach the GM tube. The interaction probability at low energy is greater than that at high energy, so the count rate decreases somewhat uniformly over the spectrum because the high energy particles travel a longer distance. The scattered electrons reaching the detector can enhance the counts at all radii, but at small radii more beta particles pass in front of the detector so more electrons reach the detector at these radii. At large radii the count rate is low so the fractional increase is higher than at small radii. Therefore, when trying to fit the data to a theoretical functional form, the counts, both for beta particles at low energies as well as those with energies near Q, have large uncertainties and can adversely affect the data analysis. To minimize these effects at large radii, students should take several counts for radii larger than the radius of the maximum energy particles (thus including scattered electrons) and take these counts as the background.

A second difficulty is that the source and detector collimators have finite widths. The source collimator has a 0.48 cm width and the detector collimator has a 0.16 cm width, so the particles enter the magnetic field over a range of ± 0.24 cm and reach the detector over a range of ± 0.08 cm, which means that the diameter is $d \pm 0.32$ cm, and the radius is $r \pm 0.16$ cm. This uncertainty in r means that when the detector is at some radius r, some particles enter the detector that have a radius of $r - 0.16$ cm. Therefore, at large radii, where the count rate changes rapidly with distance, the actual path of some of the particles is larger than the recorded radius.

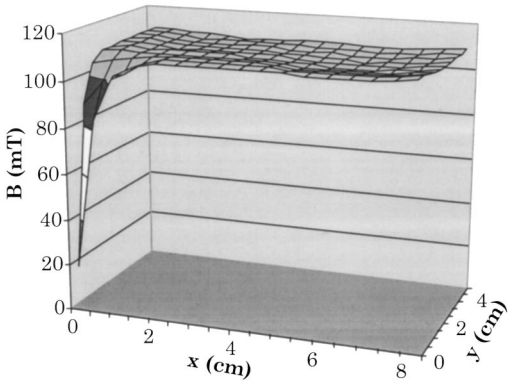

Fig. 6. Contour plot of the magnetic field between the magnets. The values are at the mid-plane between the two magnets and (0,0) (lower-left on the plot) is the location where the particles enter the magnetic field.

However, the results from data taken with a 3.2 mm collimator width give Q values for each method of analysis very similar to those found with a 0.16 cm width.

Another problem is that the magnetic field is not uniform over the entire region. The field has small variations over the path of the particles and the steel source collimator severely depresses the field near the collimator. Figure 6 shows the contour plot of the magnetic field at the location of the path taken by the particles. The magnetic field changes from 20 mT at the end of the source collimator to 105 mT at 1.0 cm from the end of the collimator. For the rest of the path, the field varies between 106 and 109 mT, with an average field of 107 mT over the path of the most energetic beta particles. The magnetic field inside the steel collimator ranges from 2 mT near the source to 7 mT at the end where the particles exit.

The source and collimator have finite widths so not all the particles come out parallel to the collimator axis. To determine the exact path of the beta particles, students can use a spreadsheet to map the path point-by-point. To determine this path, students need a good Gauss meter[12] to measure the magnetic field at 2 to 5 mm intervals along the path.

When the beta particle enters the magnetic field, it travels in a circular path with a radius of curvature equal to mv/qB, where m is the relativistic mass and v is the relativistic velocity of the particle. Figure 7 shows the particle moving

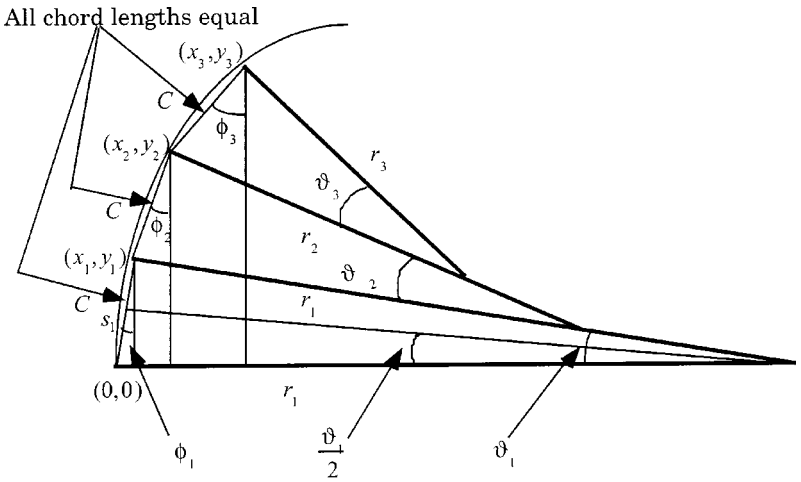

Fig. 7. Sketch of the path when the magnetic field is increasing along the particle path. The angles are determined by Eqs. (8)–(10) in the text.

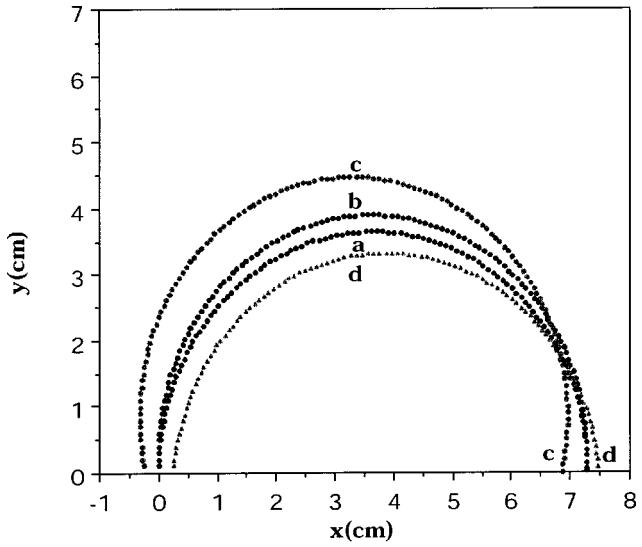

Fig. 8. Plot of the paths of 0.76 MeV beta particles (that is, maximum energy of beta particles from ^{204}Tl) generated by the spreadsheet program described in the text. Path (a) is for a uniform magnetic field and the particle exiting along the center axis of the collimator. Path (b) is a path using the actual magnetic fields along the path of the particles. Paths (c) and (d) are for particles leaving the collimator at an angle of 9° with the axis of the collimator and exiting at the front edge of the collimator.

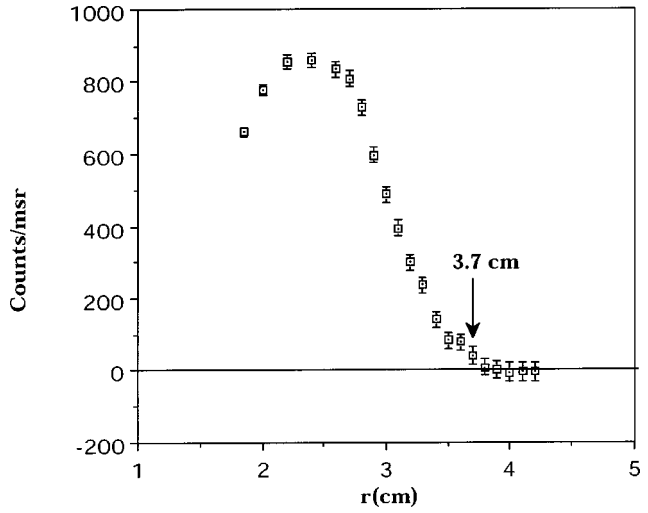

Fig. 9. Plot of data from this experiment. The values have the background subtracted from the measured values and are normalized by dividing by the solid angle subtended by the detector collimator. The arrow indicates the approximate radius (3.7 cm) where the count rate goes to zero.

through a small angle ϑ_1 while traveling an arc length s_1, where the magnetic field determines the radius of curvature at the location of the first chord. If the path increments are small, then the chord length and arc length are equal and $\vartheta = s/r = C/r$. By geometry, the angle $\phi_1 = \vartheta_1/2$ and the coordinates (x_1, y_1) are $x_1 = C \sin \phi_1$ and $y_1 = C \cos \phi_1$. As the particle travels from (x_1, y_1) to (x_2, y_2), it has a new radius of curvature determined by the magnetic field, B_2, at the second chord location. The angle,

$$\phi_2 = \vartheta_1 + \frac{\vartheta_2}{2} = \frac{\vartheta_1}{2} + \frac{\vartheta_1}{2} + \frac{\vartheta_2}{2} = \phi_1 + \frac{\vartheta_1}{2} + \frac{\vartheta_2}{2}, \tag{8}$$

determines the coordinates (x_2, y_2): $x_2 = x_1 + C \sin \phi_2$ and $y_2 = y_1 + C \cos \phi_2$. The general equations for the succeeding angles and locations are

$$\vartheta_n = \frac{C}{r_n} = \frac{CqB_n}{mv}, \tag{9}$$

$$\phi_n = \phi_{n-1} + \frac{\vartheta_{n-1}}{2} + \frac{\vartheta_n}{2}, \tag{10}$$

$$y_n = y_{n-1} + C \cos \phi_n, \tag{11}$$

$$x_n = x_{n-1} + C \sin \phi_n. \tag{12}$$

If we use Eqs. (8)–(12) and the measured values of the magnetic field, a spreadsheet can generate the beta particle positions along the entire path. Initially students enter the average magnetic field for all the locations. Then, starting at (0,0), students enter the actual magnetic field at the location of the first chord, which determines the location (x_1, y_1). Then the students enter the value of the magnetic field at the location of the second chord, which determines the location (x_2, y_2). Repeating this process generates the entire path of the particle. Figure 8 shows the different paths generated by the spreadsheet.

Path (a) is the ideal path for the particle leaving the collimator along the collimator axis and traveling though a constant 107 mT magnetic field for the entire path. The 107 mT value is the average field along the path. Path (b) is for particles leaving the collimator along the axis, but in this case the actual magnetic field values are used for each point of the path. The depressed magnetic field near the source collimator produces a path for an initial large radius. Paths (c) and (d) are for particles coming out at an initial angle (equal to that subtended by the line from the back edge of the collimator to the opposite front edge) to the collimator axis (and shifted by half the collimator width). In this case, the students add the initial angle to ϕ_1 and set the initial x-position at half the collimator width. The paths of the particles coming out at one edge of the source and initially traveling along the edge are not shown. They would be the same as path (b), but shifted by ± 0.24 cm.

Figure 8 shows that, if the detector is located at the location where the particles complete a semicircular path, the varying magnetic field and the different initial angles have little effect on the final location of the particles. Some particles originating from the right side of the source and exiting the collimator on the left side [path (c)] reach the x-axis at a distance less than most of the others; however, assuming a uniform source distribution, this fraction is small. Therefore, a nonuniform field near the collimator and particles leaving the source collimator at an angle to the axis do not significantly affect the results.

The specially manufactured aluminum GM detector did not affect the magnetic field near the detector. However, a detector with a steel casing would affect the field near the detector and hence the path of the particles as they approach the detector. With a steel ring inserted at the location of the detector, the magnetic field is 64 mT at the end of the ring (at $x = 0$) and then increases to 104 mT at a distance of 2.0 cm in front of the detector. If we substitute these magnetic field values into the spreadsheet for the path calculations, we find that a steel detector would increase the radius of the maximum energy beta particles by only 0.02 cm. Therefore, a cheaper in-stock steel GM tube would have minimal effect on the results.

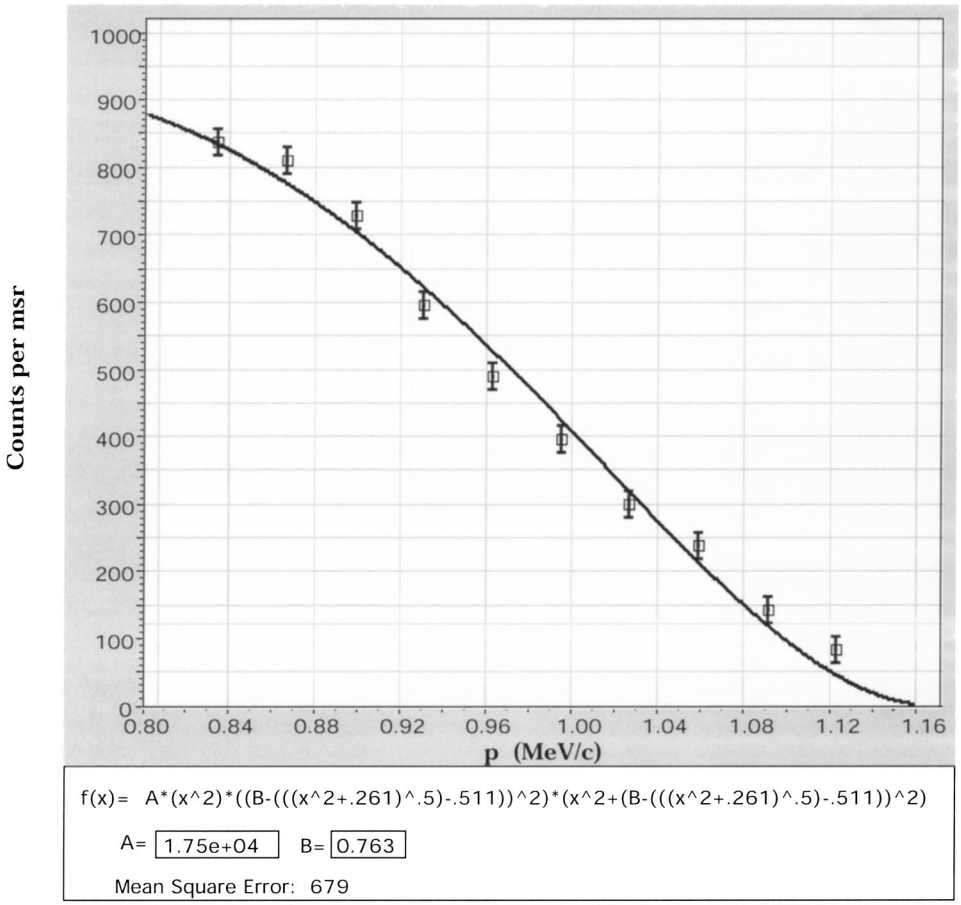

Fig. 10. Fit to the data for momentum values between 0.84 and 1.12 MeV/c. The fit gives a value of 0.76 MeV for the maximum energy of the beta particles.

V. RESULTS

Figure 9 shows data taken with the apparatus described above. Each data point represents a 20 min count, so the time needed to collect the data was more than 7 h. During a 20 min period, the 10 μCi ^{204}Tl source produced a maximum of about 3400 counts (including background) at $r=2$ cm. The background count was determined by averaging the five data points for radii greater then $r=3.8$ cm. This background consists of counts from external (natural and laboratory) sources as well as some beta particles and electrons scattered into the detector. For this experiment the background was 340 counts during the 20 min count time. All counts have background subtracted and are converted to counts per millisteradian by

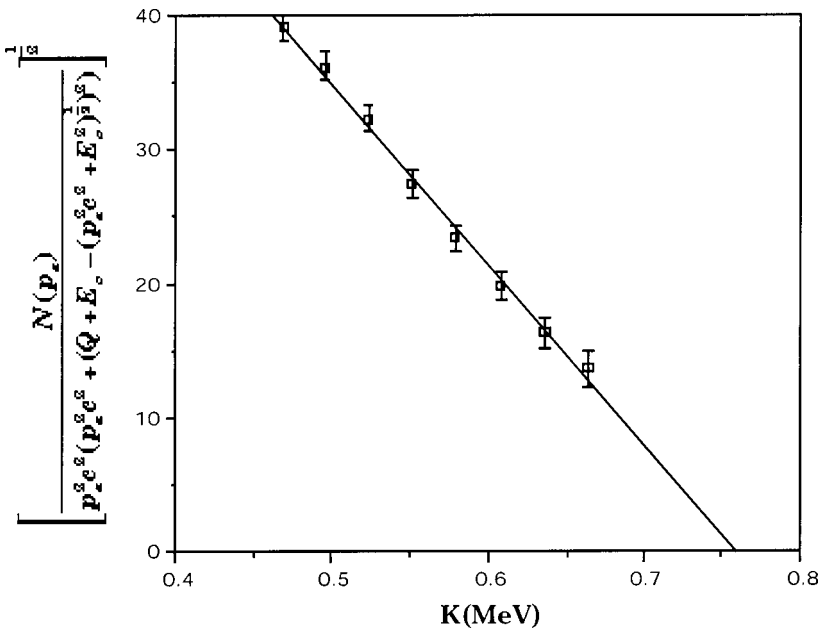

Fig. 11. Kurie plot of the data for energy values between 0.47 and 67 MeV. The equation for the fit ($y=102.4-134.9x$) gives an intercept of 0.76 MeV. The units are arbitrary because the Kurie equation is a linear relation and does not include many constants.

dividing the count by the solid angle subtended by the detector at that radius. The data are for counts every 2 mm between distances (that is, diameters) of 5.2 and 8.4 cm and every 4 mm for distances less than 5.2 cm.

Figure 9 also shows that the radius at which the counts reach zero is about 3.7 ± 0.1 cm. If we use this maximum momentum and an average magnetic field of 107 mT, the maximum beta energy is calculated to be

$$K = E - E_0 = \sqrt{(p^2c^2 + E_0^2)} - E_0 = \sqrt{[(qBrc)^2 + E_0^2]} - E_0 = 0.81 \text{ MeV}. \quad (13)$$

The magnetic field has an uncertainty of 2.5% (stated accuracy of the Gauss meter), so with this uncertainty and the 0.1 cm uncertainty in the radius, the value for the maximum energy beta particles is 0.78 ± 0.04 MeV.

To calculate the relativistic mass, students need to determine the momentum of the maximum energy beta particles and their relativistic velocity:

$$p = qrB = 1.19 \text{ MeV/c}, \quad (14)$$

and

$$p = mv = \frac{m_0 v}{\sqrt{1 - v^2/c^2}}. \quad (15)$$

The resultant velocity is

$$\frac{v}{c} = \left(\frac{p^2c^2}{m_0^2c^4 + p^2c^2} \right)^{1/2} = 0.919, \quad (16)$$

which gives a mass of

$$m = \frac{p}{v} = \frac{1.19 \text{ MeV/c}}{0.919c} = 1.29 \text{ MeV/c}^2. \quad (17)$$

Students can verify that the classical equation does not give the proper energy and velocity. Classically $K = p^2/2m$, where m is the rest mass of the electron, so the calculated energy is

$$K = \frac{p^2}{2m} = \frac{p^2c^2}{2mc^2} = \frac{(qBr)^2c^2}{2mc^2} = 1.39 \text{ MeV}, \quad (18)$$

which is considerably larger than the accepted value of 0.76 MeV. The nonrelativistic equation for kinetic energy in terms of velocity, and the kinetic energy found in Eq. (18), gives a velocity of

$$v = \sqrt{\frac{2K}{m}} = c\sqrt{\frac{2K}{mc^2}} = 2.33c. \quad (19)$$

If we use the accepted maximum energy of the beta particles, we would find $v = 1.72c$.

Figure 10 shows that the fit of the data[13] to Eq. (3) gives a $Q = 0.76$ MeV. To avoid large uncertainties in the data points near $K = Q$ and in the lower energy data, the fit includes data only from $p = 0.84$ to 1.12 MeV/c (or E = 0.47 to 0.72 MeV). By including the uncertainties in the radius and magnetic field, the value of Q derived from the fit is 0.76 ± 0.04 MeV.

Figure 11 shows the Kurie plot, which gives $Q = 0.76 \pm 0.04$ MeV. The data are limited to the region of $E = 0.47$ to 0.67 MeV to avoid large uncertainties in the data.

VI. CONCLUSIONS

The results show that the apparatus gives excellent agreement with the accepted value for the Q-value for ^{204}Tl. The fit and the Kurie plot give slightly better results than the simple extrapolation to zero counts, but even with the simple analysis, students should obtain excellent agreement with the accepted maximum energy value. The parts for the apparatus are readily available from manufacturers, but it is necessary to build the holder for the magnets, source, and detector.

ACKNOWLEDGMENT

The author thanks Rick Lindsey, the technician for the Dickinson College Department of Physics and Astronomy, for the construction of the apparatus and for helpful discussions on the design.

[1] J. Higbie, "Undergraduate relativity experiment," Am. J. Phys. **42** (8), 642–644 (1974).

[2] P. A. Egelstaff, J. A. Jackman, P. J. Schultz, B. G. Nickel, and I. K. MacKenzie, "Experiments in special relativity using Compton scattering of gamma rays," Am. J. Phys. **49** (1), 43–47 (1981).

[3] Matthiam J. H. Hoffman, "The Compton effect as an experimental approach toward relativistic mass," Am. J. Phys. **57** (9), 822–825 (1989).

[4] P. L. Jolivette and N. Rouze, "Compton scattering, the electron mass, and relativity: A laboratory experiment," Am. J. Phys. **62** (3), 266–271 (1994).

[5] Sherwood Parker, "Relativity in an undergraduate laboratory—measuring the relativistic mass increase," Am. J. Phys. **40** (2), 241–244 (1972).

[6] See for example, Kenneth S. Krane, *Introductory Nuclear Physics* (Wiley, New York, 1988), pp. 280–284.

[7] Supplied by Spectrum Techniques.

[8] LND model 72240.

[9] Magnets are available from Adams Magnetic Products (34 Industrial Way, East, Eatontown, NJ 07724, ⟨www.adams-magnetic.com⟩, and from Magnetic Component Engineering (23145 Kashiwa Court, Yorrance, CA 90505, ⟨www.magneticcomponent.com⟩).

[10] See for example, Kenneth S. Krane, *Introductory Nuclear Physics* (Wiley, New York, 1988), p. 203.

[11] See, for example, James E. Turner, *Atoms, Radiation, and Radiation Protection* (Wiley, New York, 1995), 2nd ed., p. 145.

[12] A BF. W. Bell 4048 Hand Held Gauss/Tesla meter was used for these data.

[13] Graphical Analysis by Vernier Software.